ELSEVIER

Colloids and Surfaces
A: Physicochemical and Engineering Aspects 127 (1997) 263–272

COLLOIDS AND SURFACES A

Growth, microstructure and sintering behavior of nanosized silicon powders

J. Dutta [a], H. Hofmann [a,*], R. Houriet [a], H. Hofmeister [b], C. Hollenstein [c]

[a] *Laboratoire de Technologie des Poudres, Département des Matériaux, Ecole Polytechnique Fédérale de Lausanne, CH-1015 Lausanne, Switzerland*

[b] *Max-Planck Institute of Microstructure Physics, Weinberg 2, D-06120 Halle, Germany*

[c] *Centre de Recherches en Physique des Plasmas, Ecole Polytechnique Fédérale de Lausanne, CH-1015 Lausanne, Switzerland*

Accepted 10 February 1997

Abstract

The growth and properties of nanosized silicon particles produced by gas-phase reaction in a low-pressure silane plasma has been studied. In situ ion-mass spectroscopy and Mie scattering measurements were used to monitor the formation of powders. High resolution transmission electron microscopic (HREM) studies confirmed the observations made by Raman spectroscopy that the nanoparticles grow from medium range ordered clusters. Onset of crystallization was ~700°C when structures ranging from very small crystalline ordered regions of 2.5–3.5 nm in size to fast-grown multiply twinned crystallites were formed. Size and surface roughness of the as-prepared powders were widely preserved throughout all stages of heating. It was observed that the powder morphology influences the sintering behavior. Silicon clusters which are formed during the powder synthesis acted as seeds for the crystallization process which led to the formation of polycrystalline particles. Classical sintering models offer inadequate explanation of sintering behavior, but hard-core/sinterable coating or particle sliding models can explain the sintering rate of this powder satisfactorily. © 1997 Elsevier Science B.V.

Keywords: Nanoparticles; Sintering behavior

1. Introduction

Nanophase materials, characterized by an ultra fine grain size (< 50 nm), have created great interest in recent years by virtue of their unusual mechanical, electrical, optical and magnetic properties. For example:

(1) Nanophase ceramics demonstrate enhanced ductility at elevated temperatures as compared with the coarse-grained ceramics [1].
(2) Nanosized metallic powders show cold welding properties, which, combined with the enhanced ductility, makes them suitable for metal–metal bonding especially in the electronic industry [2].
(3) Nanostructured semiconductors are known to show various nonlinear optical properties [3]. Semiconductor Q-particles also show quantum confinement effects which may lead to special properties, like the above-gap luminescence in silicon powders [4,5].
(4) Very small particles, ranging from a few atoms up to about 2 nm diameter particles, have a fully disorganized structure with discrete

* Corresponding author.

PII S0927-7757(97)00107-6

electronic states, which leads to specific properties outside the super-paramagnetism behavior [6,7]. Nanocomposites have been used for high density information storage and magnetic refrigeration [8,9].

Nanophase or cluster-assembled materials are based on creating small atomic clusters and then fusing them into a bulk material. Clusters and cluster-assembled materials are being intensively studied because of projected possibilities for the fabrication of controlled nanostructured materials [10]. These materials are being envisaged as the next-generation structural and functional materials for high technology engineering applications [11,12]. Generally, the clusters are either synthesized by wet chemical methods or by gas phase condensation methods [13].

Low temperature powder processing has been found to be suitable for the fabrication of inorganic powders. Nonthermal plasmas require small input power and flow rates whereupon the low pressure, low temperature and the increased residence time of the starting precursors in the plasma make it an interesting process for the fabrication of nanoscaled powders [14]. However, in order to control the particle sizes and distribution it is necessary to understand properly the formation and agglomeration processes in these plasmas. We have recently shown the possibility of synthesizing nanosized silicon powders by plasma-induced dissociation of silane following a route closely resembling the processing of semiconductors in microelectronics [15]. Here we will discuss about the growth of clusters in a silane plasma and the typical properties of the powders formed from these clusters. We will also discuss the dispersion and sintering behavior of these powders which could be used to expand the discussion to include the more complicated alloy systems.

2. Experimental details

The powders were prepared in a conventional capacitively coupled radio-frequency (r.f.) plasma enhanced chemical vapor deposition (PECVD) system. The reactor consists of two symmetric stainless steel cylindrical electrodes contained in a cubic vacuum vessel. The color of the powders collected varied from reddish-brown to yellow depending on the conditions of synthesis.

The clusters formed during synthesis were monitored by ion-mass spectrometry and Mie-scattering measurements. Nonperturbative anionic cluster sampling was carried out in a quadrupole mass spectrometer (Hiden), details of which are available elsewhere [16]. Polarization sensitive Mie-scattering was used to quantitatively estimate the number density and particle sizes during powder formation [17].

Annealing of the powders was carried out in forming gas (92% nitrogen and 8% hydrogen) at various temperatures (300–900°C) for 1 h or longer. Powders exhibiting a reddish-brown to yellow-orange color that changed to blackish-brown upon annealing were then transferred to carbon-coated copper grids for transmission electron microscopy inspection in a JEM 4000EX operated at 400 kV.

3. Results and discussion

In the plasma, silane is dissociated by electron impact producing neutrals (SiH, SIH_2 and SIH_3) as well as positively and negatively charged species. The polymerization proceeds through negative ion clustering in a condensation reaction [Eq. (1)] [18,19]:

$$Si_nH_x^- + SiH_4 \rightarrow (Si_{n+1}H_{x'}^-)^* + (H, H_2 \text{ products}). \quad (1)$$

where the initiating step is the formation of monosilicon hydride anions by dissociative attachment to silane, Eq. (2),

$$SiH_4 + e^- \rightarrow SiH_x^- + \{(4-x)\ H \text{ products}\}. \quad (2)$$

The formation of clusters, at least up to about 40 atoms of silicon (Fig. 1) arises from negative ion polymerization, while neutral–neutral agglomeration leads to the formation of the nanopowders.

In situ light scattering experiments were used to monitor the growth of silicon powders in the plasma. A typical example is shown in Fig. 2. The

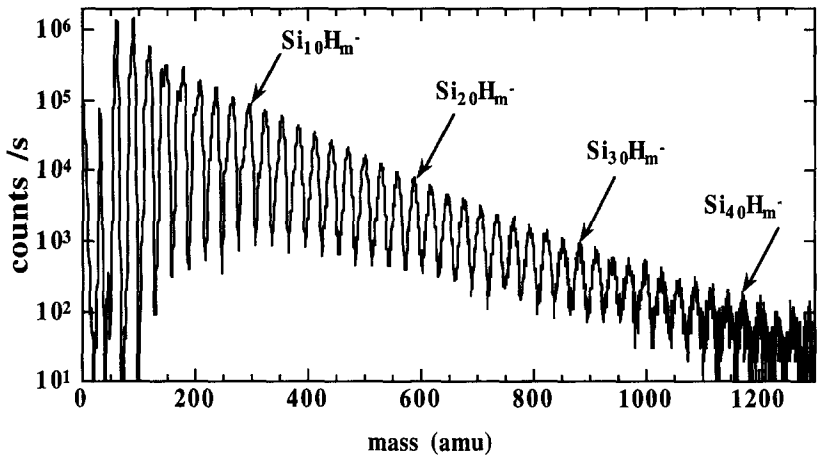

Fig. 1. Mass-spectra of the negative ion clusters in the silane plasma.

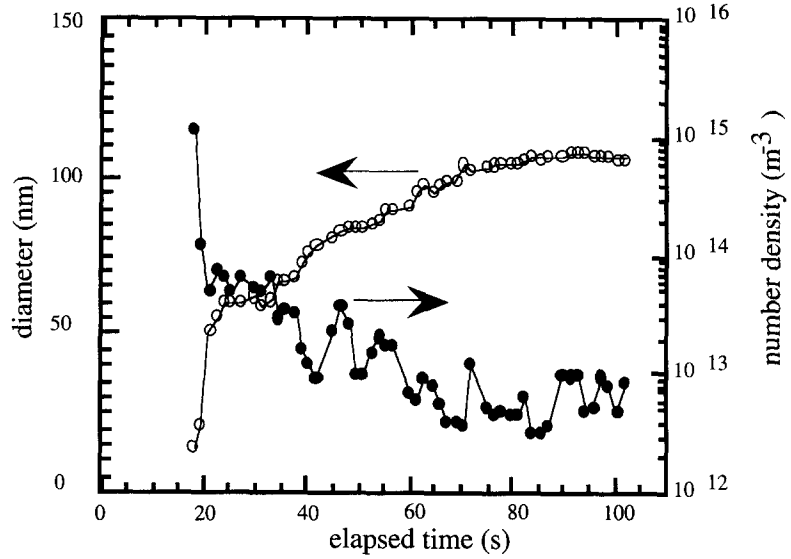

Fig. 2. Particle diameter and number density evolution profiles with respect to elapsed time after the ignition of the plasma, as determined from Mie scattering experiments.

powder formation process was found to consist of three distinct regions: the initial clustering phase, a second phase consisting of the formation of larger primary particles, and, finally, aggregation of the primary particles into agglomerates. No scattering signal could be detected in the first 17 s after the ignition of the plasma, which can be correlated to the initial stages of the negative ion formation as during this period the growth of the negative ion signal with time, as monitored by ion-mass spectroscopy, was observed. From 17–20 s, the Raleigh scattering from the particles could be used to calculate the sizes (< 30 nm). This describes the formation of the primary particles, which we observe from the TEM measurements, as discussed later. After 20 s, the number density of the particles in the plasma decreased rapidly, which was associated with a rapid increase in the particle size suggesting an agglomeration process.

The overall mechanism of homogeneous

agglomeration can be schematically represented as in Fig. 3. The limiting process for the primary particle growth can be related to the initial agglomeration phase of the negatively charged clusters while the final aggregate sizes are determined by forces experienced by the particulates in the plasma.

3.1. Microstructure

Selected area electron diffraction (SAED) during transmission electron microscopy showed halos typical of amorphous materials [20]. X-ray diffraction (XRD) patterns also showed amorphous features [21]. HREM analysis demonstrated that the powders are amorphous as no lattice fringes were observed. However, typical Raman spectra of the as-prepared powder show the optical phonon band downshifted by approximately 10 cm^{-1} as compared with bulk crystalline silicon. In some samples distinct superimposed weaker peaks were also observed and were attributed to molecular-like or localized modes [22]. Further careful observation of the HREM images showed circular contrast features, 1.5–2.5 nm in size, embedded in the amorphous particles. This was attributed to the presence of medium range order in these regions. This suggests that the precursor silicon clusters which form the particles were in the 2–3 nm range, and some of them survived even in the agglomerated form inside each particle. This nonhomogeneous atomic distribution, with partially ordered regions with dimensions of a couple of nanometers, became more pronounced upon annealing. Following our earlier Raman spectroscopic observations the HREM images further elucidated that the powder was formed from a few nanometer sized clusters (Figs. 4 and 5). Thus, a proper understanding of the cluster growth and agglomeration processes is needed in order to control the particle sizes and properties of the powders.

3.2. Dispersion

Particle size measurements of the dispersion of nanosized a–Si:H powders, obtained by plasma driven reactions of silane and silicon nitride powders (themselves obtained by laser driven reactions of silane and ammonia), suggest that the primary particles form chemically bonded aggregates which are difficult to separate. Aggregate sizes of 160 nm were observed in the silicon powder as determined by photon-correlation spectroscopy (Table 1). The

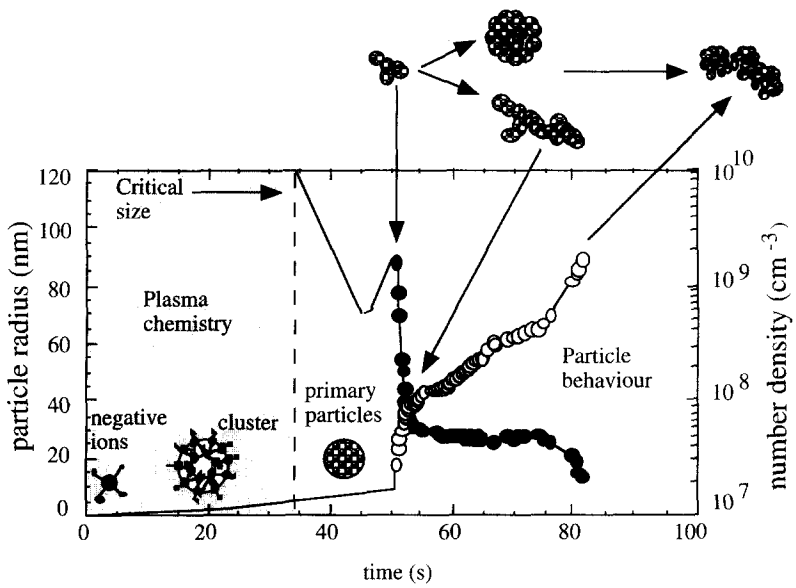

Fig. 3. Schematic representation of the particle growth in the silane plasma (not to size).

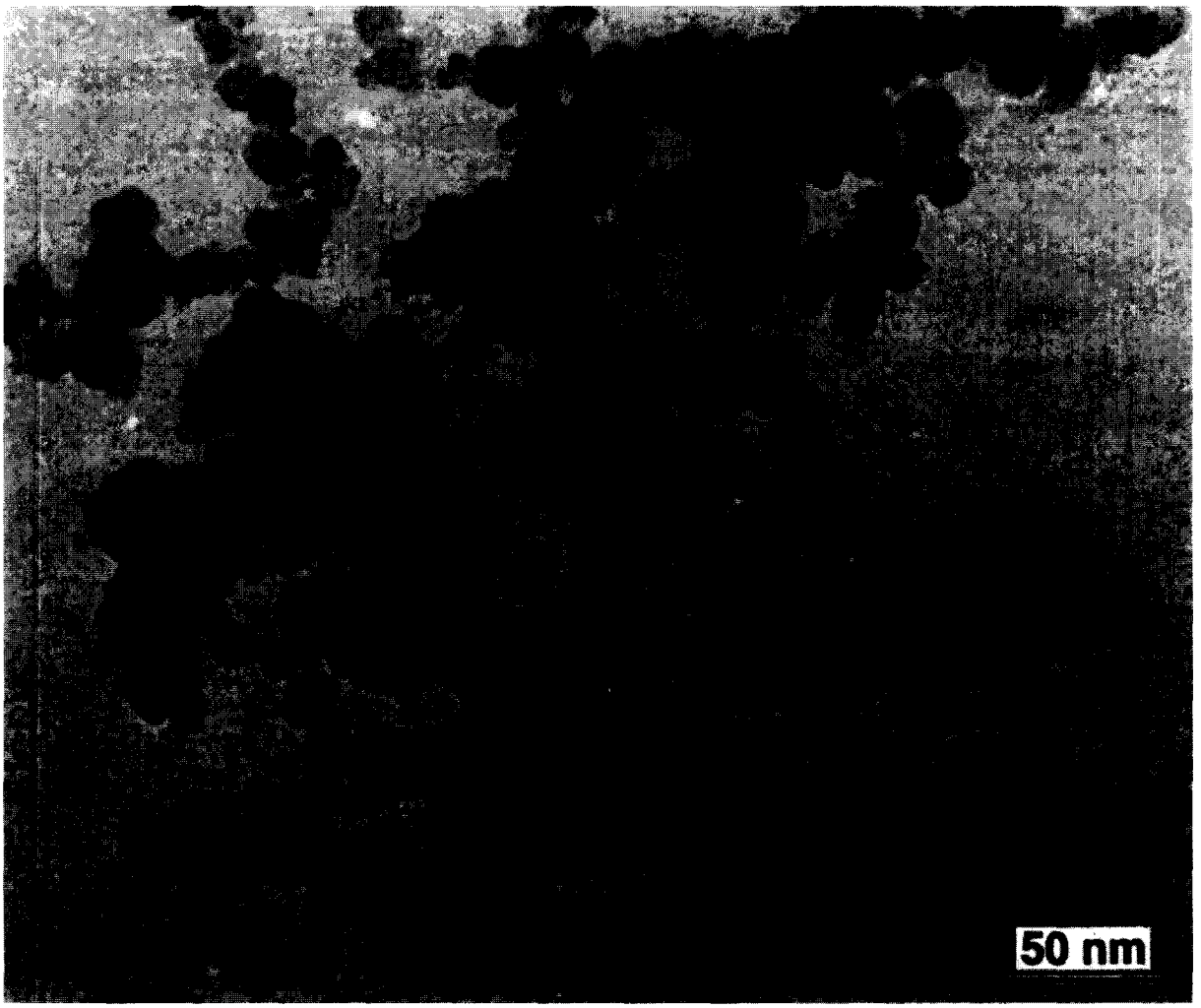

Fig. 4. TEM of typical silicon powders showing narrow size distribution of the primary particles.

silicon nitride powders obtained by laser driven reactions formed aggregates of about 500 nm, while the commercial UBE powders are dispersed in aggregates of 600 nm. This agrees well with the reported values of the particle sizes. The smaller aggregate sizes of the powders synthesized by the plasma processing could be due to the charging effects of nanometer-sized powders in the plasma.

3.3. *Annealing and sintering behavior*

Upon annealing between 300 and 600°C for 1 h, an enhancement of the circular contrast features on the scale 1.5–2.5 nm, as marked by circles in Fig. 5, is observed in the HREM images. This observation and the formation of five-fold twinned structures upon annealing at higher temperatures indicated the presence of pre-formed clusters of medium range order having noncrystallographic symmetry, which served as seeds in the amorphous-to-crystalline transition.

Prolonged annealing of the powders at 600°C (5.5 h) resulted in numerous circular contrast features in HREM images. Upon exceeding a certain size, stable crystallites may nucleate by the rearrangement of atoms at the amorphous-to-crys-

Fig. 5. Ultra High Resolution TEM of typical individual silicon particles showing ordered phases (some of these are encircled in white).

Table 1
Diameter of aggregates in different types of powders in various solvents as determined by photon correlation spectroscopy

	Ethanol	Water	Butanone-2
Si	146±11 nm	–	162±15
Si_3N_4 (ENEA)	470±30 nm	720±50 nm	530±50
Si_3N_4 (UBE 10)	650 nm	630 nm	

talline interface. Upon annealing at 700°C for 1 h, formation of distinct crystallites was observed. SAED patterns exhibited dotted rings superimposed by diffuse broad rings, which is characteristic of a low-dimensional crystalline phase in an amorphous matrix. Small-scale crystalline ordering was observed along with some fast-grown five-fold twinned crystallites. Already at this stage of crystallization growth, twinning was found to take place.

Upon annealing between 800 and 900°C, almost all particles showed an extended crystal lattice. The thermal treatment resulted in the formation of polycrystalline single particles. However, the particle size or the degree of agglomeration did not change. Despite the presence of oxygen in the as-prepared powders, rapid oxide formation could be observed only upon annealing at temperatures

of ~350°C. As is obvious by comparison of the images shown in Fig. 6, the formation of an oxide skin can be clearly seen in the HREM after annealing at temperatures as high as 700°C. At 900°C the oxide surface layer evolves to a thickness of about 2 nm. Because of the oxide layer sintering is prevented effectively, but rearrangements of the particles has been observed [4].

The sintering behavior of silicon (Si) nanoparticles is still not very well understood [23]. Si is covalently bonded with sintering temperatures between 0.75 T_m (beginning of the densification) and 0.98 T_m (maximum density). It is well known that the melting temperature (T_m) decreases with decreasing particle size: for a particle size of 17 nm the melting temperature is 95% of the melting temperature of the bulk material. This small difference of T_m should not influence the sintering behavior of the nanosized Si powders. Starting from the description of the microstructure of this system (Figs. 4 and 5) we can discuss the sintering behavior by using the model of particles with a hard but 'unsinterable' core covered by a soft sinterable layer. Following Jagota [24], for monosized, spherical, coated particles of diameter d, forming a packing with solid fraction ρ, the minimum coating thickness c, needed to achieve full density, is:

$$c/d=(1/\rho)^{1/3}-1. \quad (3)$$

In agglomerated powders with ρ of 50%, a coating thickness of 2 nm is enough for complete densification, whereas in areas between the agglomerates a coating of 5.5 nm is necessary.

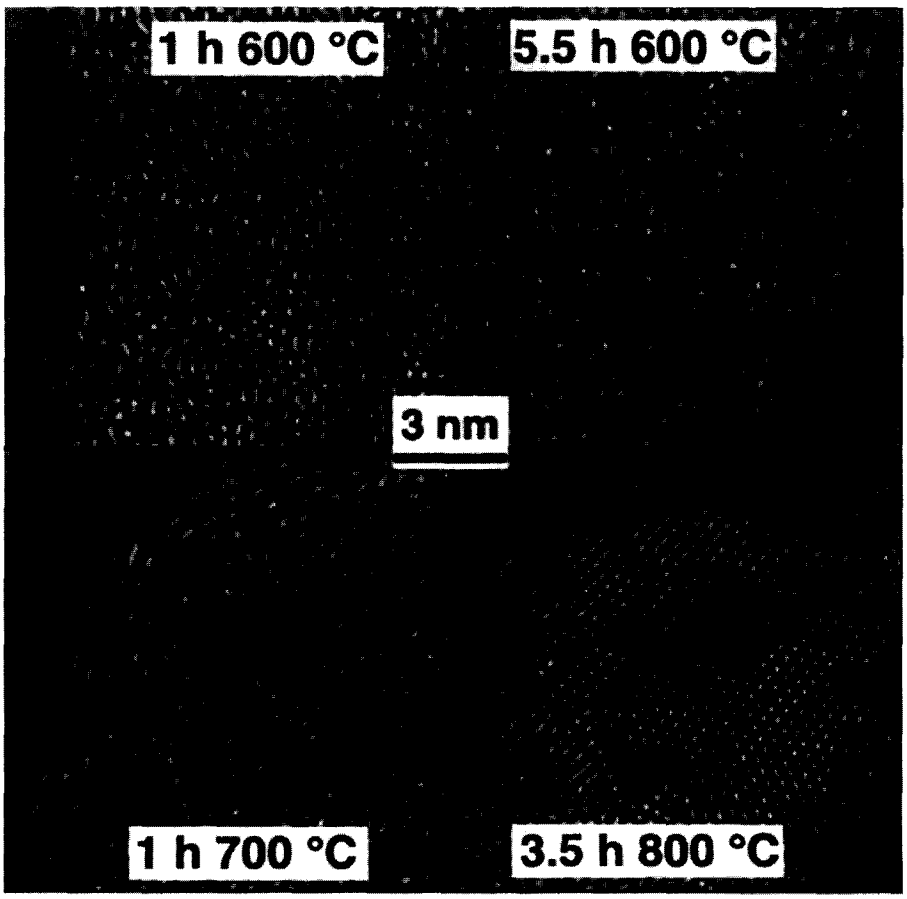

Fig. 6. Ultra-high-resolution TEM of typical individual silicon particles after annealing at different times and temperatures.

Here we will concentrate on the sintering of the agglomerates where $c=0.25d$ because only for this area is the observed coating of 2 nm enough for a full densification.

The relative density after 10 min sintering at 900°C is estimated from Fig. 4 (in [25]) using the normalized time τ' which is defined as:

$$\tau'=(3/4\pi)^{1/3}\tau\gamma/(\eta(d+c), \quad (4)$$

where τ=sintering time; γ=surface energy; and η=viscosity of the coating at the sintering temperature (for SiO_2 at 900°C, 2×10^{13} Pa s). For estimating value of the surface energy of amorphous SiO_2 nanoparticles, the following equation for their estimation was used [25]:

$$\gamma'=\gamma(1-\theta_3 a/r+\theta_4(a/r)2+\ldots), \quad (5)$$

where γ' is the surface tension of nanoparticles in J m^{-2}; θ=numerical coefficient θ_3; $\theta_4=1$; r= radius of the particles; and a=lattice constant or, in this case, the distance between the nearest neighbors.

Using 0.2 J m^{-2} for γ and 0.06 nm for a typical distance between tetrahedral SiO_4 [27], the calculated γ' for 17 nm amorphous SiO_2 particles is 0.19 J m^{-2}. With this value and a sintering time of 10 min, the change in the relative density is only 1%. These results show clearly that only limited sintering occurs (sintering time 1 month) for this mechanism (viscous flow with hard core) in the system Si/SiO_2, even in the nanosized domain at temperatures of $>0.5\ T_m$. This model thus cannot describe the observed rearrangement [24]. Therefore, a more detailed model based on the work of Gryaznov and Trusov (see, for example, [26]) was used for the explanation of the observed rearrangement. We can assume that internal plastic deformation is inhibited in Si nanoparticles especially in our case of polycrystalline particles because the critical length for dislocation will be larger than the diameter of the crystallites or the particles. Therefore, the contribution of interparticle sliding to nanopowder shrinkage becomes substantial. In the agglomerates the typical size of the pores are of the same order as the particle size. Such an ensemble of nanoparticles allows interparticle sliding where nanoparticles, as a whole, slip into pores. The driving force for such a process is the surface tension and the shrinkage rate may be described approximately by the equation:

$$d\rho/dt=D_p\gamma'\rho/kT, \quad (6)$$

where D_p=effective diffusion coefficient of nanoparticles in the agglomerate. The characteristic sintering time t' can be calculated by $t'=kT(d/a)1.5/D_p$. D_p depends upon the particle size and on the surface diffusion:

$$D_p=(a/d)^{3/2}D_s, \quad (7)$$

where $D_s=1.3\times10^{-12}$ m^2 s^{-1}, for Si nanoparticles $D_p=8.6\times10^{-16}$ m^2 s^{-1} and therefore the characteristic sintering time is <1 s. This value is comparable with the characteristic sintering time of nickel nanoparticles sintered at 600 K. These results show that the sintering of Si nanoparticles coated with SiO_2 in the agglomerates is fast at relatively high temperatures. This leads to a densification of the agglomerates, and a complete densification of the sample is impossible or possible only at very high temperatures, as observed for submicron or micron-sized Si powder. It is interesting to note that the use of the classical approach of the sintering theory to explain the sintering of Si nanoparticles gives much lower characteristic sintering times ($t'\ll1$ s) [28]. The reason for this difference is still unknown.

4. Conclusions

In the present study, we have discussed the formation of negatively charged clusters which agglomerate to form 20–30 nm-sized silicon powders by plasma-induced reactions in silane. High resolution transmission electron microscopic studies have elucidated the presence of clusters which show medium range order with noncrystallographic symmetry that gives rise to molecular-like modes observed in Raman spectra. Further work is warranted in order to understand the clustering phenomena, which will make it possible to control the primary particle sizes. The crystallization process in these powders is determined by the clusters which act as seeds for the crystalliza-

tion. The crystallization is preceded by medium-range-order formation, probably with the primary clusters formed during the powder synthesis serving as seeds. Besides small scale crystalline ordering, from the very beginning of crystallization, fast-grown five-fold twinned crystallites occur. The crystallization proceeds mainly by growth twinning, leading to a heavily faulted structure of the dc lattice.

The investigation of the sintering behavior of nanosized Si powder showed clearly that the powder morphology had a very important influence on the sintering behavior. Particles produced by a plasma process are amorphous and crystallized at half the melting temperature of the bulk material. Additionally, an amorphous silica layer on the surface of each particle was observed. The sintering behavior was determined by this silica layer. The models used, such as the hard core/sinterable coating or the model of particle sliding, can explain the sintering rate of this powder. Even at 900°C (0.63 T_m) only sintering of the agglomerates was observed, whereas the sintering of the sample was negligible. The use of a classical model to explain the sintering process was not successful.

These powders should be useful for the preparation of reaction-bonded silicon nitride as the reaction with nitrogen is expected to occur at lower temperatures due to the small particle sizes 29. Further detailed work is necessary to understand the growth of these clusters in the plasma, and hence to control the primary particle sizes [29]. This will enable us to fabricate other silicon alloys (like silicon nitride, silicon carbide, etc.) using this process.

Acknowledgment

The authors are thankful to Dr A.A. Howling and Mr C. Bossel for some measurements. This work was partially supported by Swiss Federal Grants FN 2100-039361.93/1 and EF-REN (93) 35 and BBW.93.0136 (for Brite-Euram contract BE-7328).

References

[1] T.G. Nieh, J. Wadsworth, F. Wakai, Int. Mat. Rev. 36 (1991) 146–161.
[2] H. Eifert, B. Günther, Proc. Powder Metallurgy World Congress, Paris, 6–9 June 1994, European Powder Metallurgy Association, France, 1994, p. 1801.
[3] J.H. Fendler (Ed.), Membrane-mimetic approach to advanced materials, in: Advances in Polymer Science 113, Springer, Berlin, 1994.
[4] J. Dutta, R. Houriet, C. Hollenstein, H. Hofmann, in: P. Jena (Ed.), Clusters and Nanostructured Materials, Nova Science Inc., New York, 1997, in press.
[5] C. Courteille, J.-L. Dorier, J. Dutta, C. Hollenstein, A.A. Howling, J. Appl. Phys. 78 (1995) 61.
[6] J.L. Dorman, Mat. Sci. Engng A168 (1993) 217.
[7] M.J. Aus, B. Szpanar, V. Erb, G. Palumo, K.T. Aust, Mat. Res. Soc. Symp. Proc. 318 (1994) 39.
[8] J.C. Parker, R.W. Siegel, Nanostructured Mat. 1 (1992) 53.
[9] R.D. Shull, L.E. Bennett, Nanostructured Mat. 1 (1992) 83.
[10] NATO ASI series C, Mathematical and Physical Sciences, vol. 374, Physics and Chemistry of Finite Systems: From Clusters to Crystals, P. Jena, S.N. Khanna, B.K. Rao (Eds.), Kluwer, Dordrecht, 1992.
[11] A.J. Burggraaf, A.J.A. Winnubust, H. Verweij, Proc. Third Euro-Ceramics 3 (1993) 561.
[12] R. Roy, in: S. Komarneni, J.C. Parker, G.J. Thomas (Eds.), M.R.S. Symp. Proc., vol. 286, Materials Research Society, Pittsburg, 1993, p. 241.
[13] R.W. Siegel, Nanostructured Mat. 4 (1994) 121.
[14] H. Drost, H.-D. Klotz, R. Mach, K. Szulzewsky, in: N. Mizutani et al. (Eds.), Advanced Materials '93, Trans. Mat. Res. Soc. Jap., 14A (1994) 53.
[15] J. Dutta, R. Houriet, H. Hofmann, J.-L. Dorier, A.A. Howling, C. Hollenstein, in H.J. Mathieu, B. Reihl and D. Briggs (Eds.), Proc. of ECASIA '95, Wiley and Sons, Chichester & New York, 1996, p. 483.
[16] A.A. Howling, C. Courtielle, J.-L. Dorier, L. Sansonnens, C. Hollenstein, J. Pure Appl. Chem. 68 (1996) 1017.
[17] C. Hollenstein, J.-L. Dorier, J. Dutta, L. Sansonnens, A.A. Howling, Plasma Sources Sci. Technol. 3 (1994) 278.
[18] A.A. Howling, L. Sansonnens, J.-L. Dorier, C. Hollenstein, J. Appl. Phys. 75 (1994) 1340.
[19] K. Raghavachari, Advances in Metal and Semiconductor Clusters, vol. 2, JAI Press, Greenwich, CT, 1994, p. 57.
[20] H. Hofmeister, J. Dutta, H. Hofmann, Phys. Rev. B 54 (1996) 2856.
[21] J. Dutta, I.M. Reaney, C. Bossel, H. Hofmann, Nanostructured Mat. 6 (1995) 493.
[22] J. Dutta, W. Bacsa, C. Hollenstein, J. Appl. Phys. 77 (1995) 3729.
[23] C. Bossel, J. Dutta, R. Houriet, J. Hillborn, H. Hoffman, Mat. Sci. Engng. A 204 (1995) 107.

[24] H. Hofmann, J. Dutta, in R.M. German, G.L. Messing and R.G. Comwall (Eds.), Sintering Technology, Marcel Dekker, New York, 1996, p. 101.
[25] A. Jagota, Simulation of the viscous sintering of coated particles, J. Am. Ceram. Soc. 77 (8) (1994) 2237.
[26] V.G. Gryaznov, L.I. Trusov, Size effects in micromechanics of nanocrystals, Prog. Mat. Sci. 37 (4) (1993) 289.
[27] R.K. Iler, The Chemistry of Silica, Wiley, New York, 1979.
[28] F.E. Kruis, K.A. Kusters, S.E. Pratsinis, Aerosol Sci. Technol. 19 (1993) 514.
[29] S. Onaka, P.D. Funkenbusch, in: Properties of Emerging P/M Materials, compiled J.M. Capus, R.M. German, Proc. 1992 Powder Metallurgy World Congress, vol. 8, 1992, p. 33.